4-24-2015

A Study Of Thunderstorm Microphysical Properties And Lightning Flash Counts Associated With Terrestrial Gamma-Ray Flashes

D. E. Barnes

Michael E. Splitt

Joseph R. Dwyer

Steven M. Lazarus

David M. Smith

See next page for additional authors

Authors

D. E. Barnes, Michael E. Splitt, Joseph R. Dwyer, Steven M. Lazarus, David M. Smith, and Hamid K. Rassoul

AGU PUBLICATIONS

JGR

Journal of Geophysical Research: Atmospheres

RESEARCH ARTICLE
10.1002/2014JD021495

Key Points:
- Hydrometeor characteristics of TGF thunderstorms
- Hydrometeor characteristics of non-TGF storms
- TGF-related storms have higher hydrometeor content

Correspondence to:
D. E. Barnes,
barnesd2003@my.fit.edu

Citation:
Barnes, D. E., M. E. Splitt, J. R. Dwyer, S. Lazarus, D. M. Smith, and H. K. Rassoul (2015), A study of thunderstorm microphysical properties and lightning flash counts associated with terrestrial gamma-ray flashes, *J. Geophys. Res. Atmos.*, *120*, 3453–3464, doi:10.1002/2014JD021495.

Received 16 JAN 2014
Accepted 23 MAR 2015
Accepted article online 26 MAR 2015
Published online 24 APR 2015

A study of thunderstorm microphysical properties and lightning flash counts associated with terrestrial gamma-ray flashes

D. E. Barnes[1], M. E. Splitt[2], J. R. Dwyer[3], S. Lazarus[2], D. M. Smith[4,5], and H. K. Rassoul[1]

[1]Geospace Physics Laboratory, Physics and Space Science Department, Florida Institute of Technology, Melbourne, Florida, USA, [2]Department of Marine and Environmental Sciences, Florida Institute of Technology, Melbourne, Florida, USA, [3]Space Science Center (EOS) and Department of Physics, University of New Hampshire, Durham, New Hamspire, USA, [4]Santa Cruz Institute for Particle Physics and Physics Department, University of California, Santa Cruz, California, USA, [5]Space Sciences Laboratory, University of California, Berkeley, California, USA

Abstract The terrestrial gamma ray flash (TGF) is an emission of highly energetic radiation produced by or at least in close association with lightning. Previous investigations attempted to isolate the production mechanisms and production altitude(s) of TGFs as well as macrophysical characteristics, while thunderstorm microphysical characteristics were largely ignored. This investigation into thunderstorms and their hydrometeor and flash characteristics utilize temporal and spatial coincident satellite passes between the Reuven Ramaty High Energy Solar Spectroscopic Imager and the Tropical Rainfall Measuring Mission to determine the bulk (or footprint) microphysical properties of two types of study events, the thunderstorm complexes which are associated with TGFs (TGF case) and the thunderstorm complexes which did not produce a TGF detected by Reuven Ramaty High Energy Solar Spectroscopic Imager during the pass (non-TGF case). Results are presented for two different comparison methods. The first case utilizes geographic region weighted by TGF distribution, and the second is based on TGF percentage of occurrence when compared to total flash count of data set. Results show that the associated storms around the TGF location possess differences in the hydrometeor concentrations: cloud liquid water, cloud ice, precipitation water, and precipitation ice. These results take place at different levels of the atmosphere, including the mixed phase region. Additionally, results will show that TGFs are a consistent percentage of observed flashes as the rate of TGFs as a function of Lightning Imaging Sensor flash count is relatively constant.

1. Introduction

The terrestrial gamma ray flash (TGF) has a brief yet fascinating history. A TGF is a high-energy emission of gamma rays produced within the Earth's atmosphere and usually detected at satellite altitudes. The phenomenon was first reported in 1994 [*Fishman et al*., 1994]. TGFs have been recorded on the ground [*Dwyer et al*., 2004, 2012] and from aircraft [*Smith et al*., 2010]. This form of energetic radiation, first predicted in 1925 [*Wilson*, 1925a, 1925b], was discovered by the Compton Gamma-Ray Observatory (CGRO). CGRO was designed to study astrophysical gamma ray sources. A portion of the gamma ray data returned to Earth from CGRO contained events with millisecond durations, hard spectra, and energy ranges extending above several hundred keV. Analysis eventually led *Fishman et al*. [1994] to conclude that gamma ray flashes were not of extraterrestrial origin; rather, they emanated from Earth. The initial investigation and subsequent results incorrectly concluded that these were atmospheric discharge phenomena occurring at altitudes of 40–80 km and possibly associated with Sprites, large-scale electric discharges above thunderclouds. The observed TGF spectra are composed of high-energy photons, which imply a bremsstrahlung source mechanism, involving energetic electrons. Furthermore, these TGFs appeared to be collocated within regions of the Earth with extensive thunderstorm activity.

The existence of TGFs has opened new areas of high-energy atmospheric physics research. In 2004, Dwyer et al. reported a gamma ray burst at ground level during the initial stages of rocket-triggered lightning. The gamma ray burst had an energy spectrum and time duration similar to TGFs. *Cummer et al*. [2005] found 13 TGFs that were linked to lightning discharges as measured by the extremely low frequency/very low frequency sensors, and all 13 were related to positive intracloud (+IC) discharges.

Smith et al. [2005] reported that the NASA Small Explorer Class satellite, Reuven Ramaty High-Energy Solar Spectroscopic Imager (RHESSI), also recorded TGFs with energies extending to 20 MeV with durations of 0.2–3.5 ms. *Dwyer and Smith* [2005] reported a Monte Carlo simulation which produced a series of altitude-varying modeled spectra and compared results to the RHESSI TGF spectrum. They determined that the TGF source altitude was between 15 and 21 km. *Cummer et al*. [2005] found that charge moments were too small to be associated with Sprites. The measured lightning charge moment changes in these strokes were 50–500 times smaller than seen with Sprites and 2 orders of magnitude smaller than what high-altitude Relativistic Runaway Electron Avalanche (RREA) theory predicted. *Cummer et al*. [2005] also identified that positive intracloud (+IC) discharges occurred within 300 km of the RHESSI subsatellite point, further constraining the TGF source location.

Inan et al. [2006] found that 76% of TGFs occur in association with lightning-generated radioatmospherics (sferics) arriving from near the footprint of RHESSI and within a few milliseconds of the TGF. *Grefenstette et al*. [2009] found no detectable change of the TGF spectrum when grouped by brightness (intensity), location, geomagnetic latitude, or local day/night.

Shao et al. [2010] presented results based on RHESSI-observed TGFs that found that TGFs are more likely related to small rather than large lightning pulses and intracloud flashes that transport electrons upward within the cloud. Additionally, *Shao et al*. [2010] estimated the heights of the TGF production level to be in the range of 10.5–14.1 km, within the thunderstorm cloud and not above it. *Xu et al*. [2012] reported that location of intracloud discharges responsible for TGF emission occurred at an altitude range of approximately 10 km. *Smith et al*. [2011] observed a TGF utilizing the Airborne Detection for Energetic Lightning Emission. This TGF event was only the second known TGF observed within the atmosphere; at approximately ~14 km, *Dwyer et al*. [2012] reported a second ground level TGF measured at the International Center for Lightning Research and Testing. These investigations helped identify how TGFs may be initiated; however, the association of TGFs to lightning and the thunderstorm remains an enigma.

The production mechanism behind TGFs is thought to be based on the Relativistic Runaway Electron Avalanche (RREA) mechanism [*Wilson*, 1925a, 1925b; *Gurevich et al*., 1992; *Roussel-Dupré and Gurevich*, 1996; *Gurevich and Zybin*, 2001; *Dwyer*, 2003]. Atmospheric discharges may also be described by runaway electron production in the high electric fields associated with lightning leaders or streamers [*Moss et al*., 2006; *Dwyer*, 2008; *Carlson et al*., 2010] and by the relativistic feedback discharge mechanism [*Dwyer*, 2003, 2008, 2012; *Liu and Dwyer*, 2013]. These mechanisms provide a theory of how energetic electrons are produced, however do not provide a complete explanation of why some thunderstorms produce TGFs while others do not.

Splitt et al. [2010] performed the first meteorological comparison of TGFs and associated thunderstorms and reported that TGFs follow diurnal, seasonal, and geographic patterns similar to thunderstorms. Utilizing IR data, they found that TGF storm systems are closely associated with tall (13.6–17.3 km) tropical thunderstorm systems; additionally, the horizontal extent of TGF-related storms ranges in size by several orders of magnitude. *Splitt et al*. [2010] identified a specific storm/TGF event that occurred in the Mozambique Channel. The storm was analyzed utilizing Tropical Rainfall Measuring Mission (TRMM) Microwave Imager (TMI) hydrometeor 2A12 data products. The TGF storm was found to have relatively high concentrations of hydrometeors near 6 km, which is within the mixed phase region, but not atypical for tropical convection.

In this study, RHESSI subsatellite locations within regions of frequent thunderstorm activity and TGF emissions will be compared to TRMM orbital data for geospatial matches. These geospatial matches lay the foundation for the analysis of the TRMM TMI hydrometeor data. The analysis was performed on TGF-related thunderstorms and the non-TGF thunderstorms sets as recorded by RHESSI in order to identify outstanding characteristics and identify statistically significant differences between the two storm sets. Thunderstorms are classified as non-TGF, producing if no TGF was recorded by RHESSI as it passed over the storms. However, it is possible that the thunderstorms did produce TGF(s) at times when RHESSI was not overhead. Analysis will include the hydrometeor and flash characteristics of thunderstorms, which are within the field of view (FOV) of TRMM and which coincide within the pass of RHESSI for that geographical location. Do the mixed phase regions within the TGF storm contain more water and/or ice that may

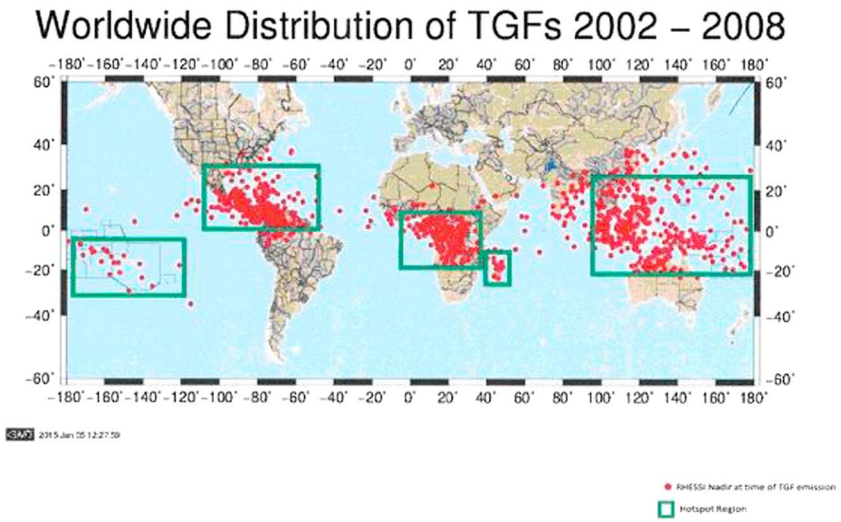

Figure 1. Worldwide distribution of all RHESSI-observed TGFs 2002–2008. Hot spots, regions of intense TGF occurrence are shown within the search boxes.

enhance electrification? Do the TGF storm complexes have a higher total flash count? These characteristics will be identified with each case and statistical analysis performed.

TGFs recorded by RHESSI have been linked to geographic regions of thunderstorm activity in the tropics. Five TGF geographic hot spots have been defined based on this observed TGF density. These locations are central Africa, Madagascar, Oceania (Southeast Asia, Malaysia south to northern half of Australia), South Pacific, and the Yucatan (including all of Central America, the southern U.S., and South America north of the South Atlantic anomaly); see Figure 1. With the exception of the small area of the northern region of South America, the RHESSI spacecraft goes into a safe mode (auto shutdown of sensitive electronic components) to protect its electronics from radiation hazards, and therefore, RHESSI may have missed TGFs which may have occurred over South America.

2. Instrumentation

The only instrument on board RHESSI is an imaging spectrometer with the ability to obtain images of solar flares in X-rays and gamma rays as a function of energy and time. The imager package consists of nine, segmented, hyper-pure germanium crystals. Germanium detectors cover the entire hard X-ray (3 keV) to gamma ray energy range (up to ~20 MeV). Detectors record the TGFs as the gamma rays penetrate the vehicle. Other than the spacecraft position, RHESSI contains no instrumentation to locate the TGF or the thunderstorm generating the TGF. RHESSI detectors are oriented toward the Sun. With respect to the Earth, the direction of the detectors will sometimes face away; sometimes, they are side on, and at midnight, the instrument points toward the Earth. Due to the varying orientation of the spacecraft, the likelihood of detecting the TGF is independent of orientation angle.

The Tropical Rainfall Measurement Mission (TRMM) is an Earth-observing science mission dedicated to study the tropical zones of the Earth. The mission is a joint venture between the National Aeronautics and Space Administration (NASA) and the Japan Aerospace Exploration Agency. According to the document Tropical Rainfall Measuring Mission (TRMM) Sensor Package [*Goddard Space Flight Center* (*GSFC*), *NASA*, 1998], the sensor package consists of the TRMM Microwave Image (TMI), visual and infrared scanner, precipitation radar (PR), Cloud and Earth's Radiant Energy System, and the Lightning Imaging Sensor (LIS).

TRMM Microwave Image (TMI) utilizes a passive microwave sensor aimed earthward to provide detailed rainfall information over a wide path beneath the TRMM satellite (http://science1.nasa.gov/missions/trmm/, 2013). The most important feature of the TMI in regards to this research is its ability to provide vertical profiles of the associated hydrometeors from the surface up to a height of about 20 km. The TMI instrument measures very small amounts of the microwave energy emitted by the Earth and the

Table 1. TRMM Microwave Imager 14 Vertical Profile Layers[a]

Layer Index	Layer Height
0	surface–0.5 km
1	0.5–1.0 km
2	1.0–1.5 km
3	1.5–2.0 km
4	2.0–2.5 km
5	2.5–3.0 km
6	3.0–3.5 km
7	3.5–4.0 km
8	4.0–5.0 km
9	5.0–6.0 km
10	6.0–8.0 km
11	8.0–10.0 km
12	10.0–14.0 km
13	14.0–18.0 km

[a]Table courtesy of NASA Goddard Space Flight Center.

atmosphere. The TMI instrument is able to infer such quantities as hydrometeor concentration in the atmosphere and near the Earth's surface (http://science1.nasa.gov/missions/trmm/, 2013). The TMI sensor measures the magnitude of radiation at five spectral frequencies: 10.7, 19.4, 21.3, 37.0, and 85.5 GHz. TMI data are recorded in a path of 878 km with a resolution at the Earth's surface of 5.1 km at 85.5 GHz (highest resolution) [*GSFC*, *NASA*, 1998]. The other four frequencies are considered low resolution. The hydrometeor content is disseminated at 14 levels. Table 1 lists the relation between level and altitude. TRMM data products used in this research are derived from the TMI profiling algorithm (2A12). According to the TRMM 2A12 Readme file [*Bonk*, 2008] provided by NASA Goddard Earth Sciences Data and Information Services Center (GES DISC), "The TMI profiling algorithm (2A12) generates vertical profiles of hydrometeors latent heating from TMI brightness temperatures by blending the radiometric data with dynamical cloud models. For each pixel, the algorithm assigns a surface type (land/ocean/coast) and a freezing height and computes surface rain, convective surface rain, and profiles of hydrometeors (cloud liquid, cloud ice, water vapor, etc.) and latent heating at 14 vertical levels." The TMI hydrometeor data are distributed as the data product: 2A12 version 6. The 2A12 V6 data set will be used to profile the hydrometeor content of the storm sets under study. Version 6 2A12 data are utilized as version 7 data had not been made publicly available at the start of this investigation. The TMI algorithms are not perfect; there is an overestimation of rainfall rates over Africa, differences due to the land versus ocean algorithms, scattering or radiance measurements by hydrometeors which lead to higher rainfall rates, and the larger footprint of the TMI that can reduce resolution versus the precipitation radar [*Masunaga et al*., 2002; *Wang et al*., 2009]. These deficiencies would be of major concern if comparing to ground-based measurements or TRMM PR precipitation measurements. Additionally, surface and convective rain rates generated as a data product from the TMI, which have large inconsistencies, are not presented.

The Lightning Imaging Sensor (LIS) is an optical sensor sensitive to flashes within the cloud in its field of view (FOV). At maximum observation time, LIS observes a location for 83 s. According to the *Algorithm Theoretical Basis Document for the Lightning Imaging Sensor (LIS)* (2000), the "LIS observes differing levels of lightning defined as events to areas. Events record single pixels that are brighter than the background level for a single frame, 2 ms. The largest observation is the area. An area is a continuous section observed by the LIS that has produced lightning during a single orbit with no more than a 3 pixel separation (16.5 km) between clusters of pixels." For a complete review of the TRMM electronics package, see *Kummerow et al*. [1998], *Mach et al*. [2007], and *Christian et al*. [1998].

TRMM 2A12 V6 and LIS V4 data utilized in this investigation were retrieved from the Global Hydrology and Climate Center and the Global Hydrology Resource Center both of Marshall Spaceflight Center (http://mirador.gsfc.nasa.gov/), NASA, Huntsville, AL, and Goddard Earth Sciences Data and Information Services Center (GES_DISC, http://lightning.nsstc.nasa.gov/), Goddard Space Flight Center, NASA, Greenbelt, MD. RHESSI TGF data and RHESSI orbital flight data are retrieved from the Physics Department and Santa Cruz Institute for Particle Physics, University of California, Santa Cruz, California.

3. Case Definition

This research focuses on properties of TGF-producing storm complexes as compared to the non-TGF data. The data set spans 6 years—2002 through 2008. In the time from 2008 until the present, advances in

Table 2. YES and NULL Criteria: Criteria That Must Be Met in Order to Classify a Thunderstorm as a TGF Case or Non-TGF Case Event

Condition For Event Type	TGF	Non-TGF
Lightning present	X	X
TRMM and RHESSI overlap within 500 km	X	X
TRMM RHESSI pass within ±1 h	X	X
TGF observed	X	

detection technology have been made; the FERMI [*Briggs et al.*, 2010] and AGILE [*Marisaldi et al.*, 2010] satellites are two such examples. Advances in detecting weaker TGFs within the older RHESSI data have been made [*Gjesteland et al.*, 2012] too. This data set is composed of only those TGFs that were obtained from the publicly available RHESSI data at the University of California, Santa Cruz, website. *Gjesteland et al.*'s [2012] detected weaker TGFs are not included.

Figure 1 depicts the worldwide distribution of all known TGFs through December 2008. In this graphic, TGFs are seen clustering within certain regions of the Earth. These regions will be categorized into five bins: central Africa, Madagascar, Oceania, South Pacific, and Yucatan.

The breakdown by geographic location will investigate regional meteorological characteristics of these TGF associated storms.

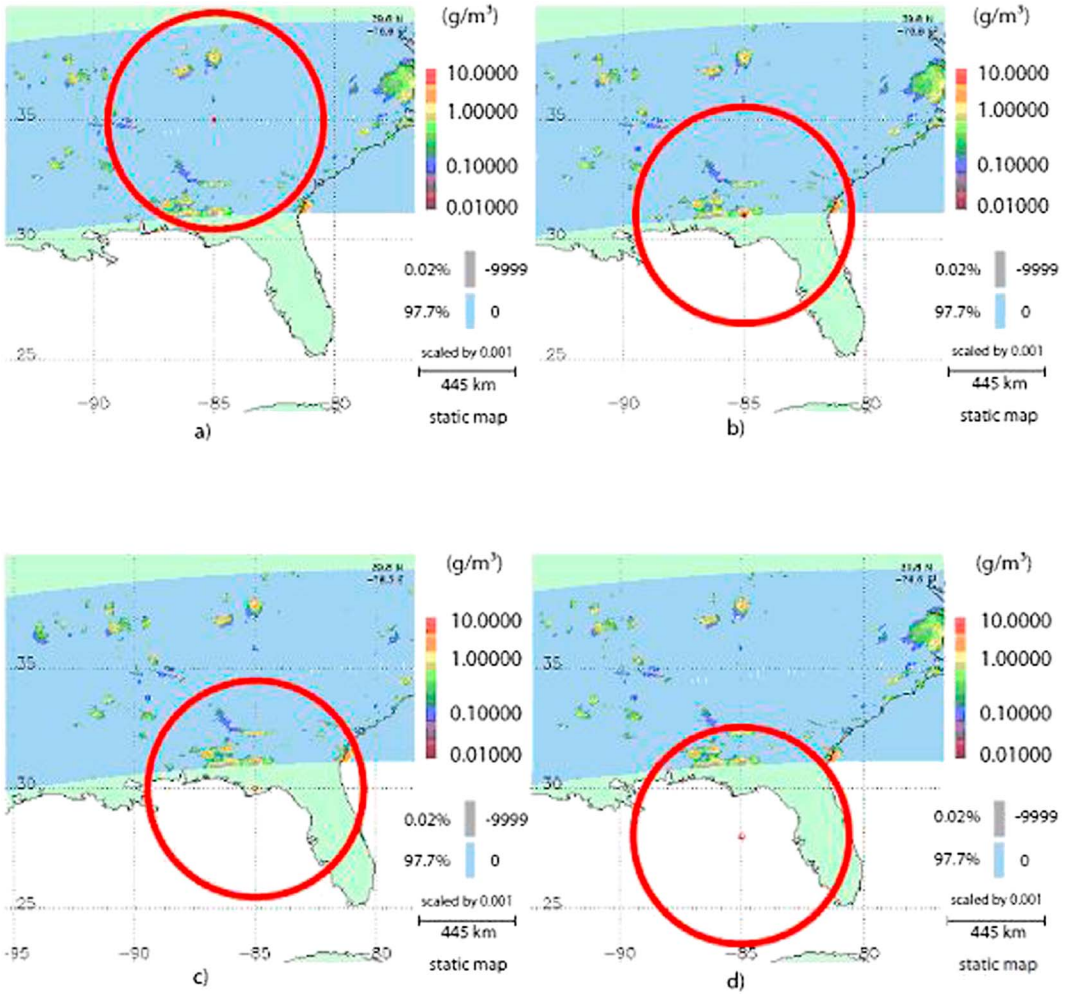

Figure 2. Schematic representation of RHESSI footprint overlap (red circle) with TRMM footprint. (a) Ideal case where the nadir positions are very close, (b) nadir positions are 500 km or less apart, and (c and d) nadir positions are greater than 500 km and are discarded. Graphics generated by the TRMM Orbit Viewer software: http://pps.gsfc.nasa.gov.

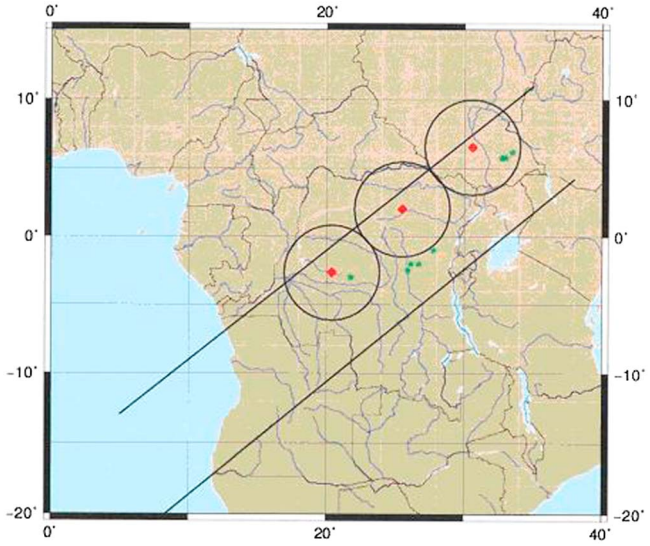

Figure 3. Three RHESSI nadir positions represented by the red diamonds (diamonds correspond to an ascending orbit) that overlap within the edges of the TRMM LIS footprint (black lines). LIS-observed lightning is depicted by the green star overlays. Each red diamond is encircled with the 500 km footprint of the RHESSI satellite (black circle). The RHESSI footprint overlaps LIS-observed lightning flashes in both the first and last footprints. The RHESSI spacecraft recorded no TGF discharge during this pass, qualifying two of the three positions as a non-TGF event.

Two cases underlie the focus of this research, the TGF case and the non-TGF case. Four conditions are applied to categorize an event as either a TGF case or a non-TGF case. Table 2 outlines the requirements.

The data collection started with the TRMM LIS identifying worldwide lightning events from January 2002 to December 2008. This selection process precludes any bias from being applied by selecting all storms within the TRMM field of view. RHESSI and TRMM orbital data were then compared within this set to identify time/date when the two satellites were over the same locations and within 500 km of each other. World Wide Lightning Location Network (WWLLN) data were investigated to try to locate the actual emitting storm; however, no matches with WWLLN data and TRMM/RHESSI matches were found. Figure 2 shows one particular example of RHESSI's footprint (red circle) and the path swept out by the TMI.

Figure 2a is the ideal case, nearly perfect overlap. Figure 2b is the maximum acceptable difference of 500 km between the two satellites nadir positions. Figures 2c and 2d show the reader examples outside the limits. Figure 3 represents a non-TGF case in which RHESSI positions are overlaid on the TRMM track. The three successive red diamonds are each separated by 150 s (approximately 1000 km).

The 150 s moves the footprint approximately 1000 km so that overlap with the previous RHESSI position does not occur. The TRMM LIS detected flashes are shown as green star overlays. The first (lower left) RHESSI position will be a data set within the non-TGF case, as is the third position (upper right). Both of these RHESSI footprints contain the TRMM LIS-observed lightning, while the middle RHESSI footprint has lightning outside the 500 km footprint.

The data set is filtered to satisfy a temporal difference of no more than 60 min. Sixty minutes was chosen for two reasons: first, it provided a data set of more than 100 TGF cases. When 30 min, 10 min, or 5 min deltas were used, few TGFs came from these reductions and not enough for any meaningful statistical comparison. The second reason relates to the thunderstorm's life expectancy and drift. For large systems, this may not be true, but on average, it may be applied. A pulse storm may last 20–30 min; therefore, the 60 min requirement would fail here. A large storm, multi-cell storm, mesoscale storm, or a squall line may last for hours [*Grenci and Nese*, 2002, chap. 8; *Burroughs et al.*, 2000, p. 49; www.crh.noaa.gov, 2014].

The first method utilizing TGF case and non-TGF case hydrometeor content detailed regional only contributions. The averaging of regional content was investigated to filter out pronounced hydrometeor differences at the highest level. The maximum concentrations were used, as they are more reflective of the interior core of the storm and the mixed phase region. Additionally, using the maximum hydrometeor content reduces the contribution from smaller events such as showers and decaying storms. TGF emission, though, has been observed after peak ice concentrations [*Smith et al.*, 2010], and in association with small storms, even when larger storms were in the vicinity [*Splitt et al.*, 2010]. Furthermore, the TRMM TMI algorithm may have impacted the results of central Africa by producing elevated hydrometeor content. This effect would be consistent through both the TGF case and non-TGF case; however, it would influence the total data set when comparing it to the oceanic regions used within this data set. The resulting data set now matches three of the criteria. The next step

Table 3. TGF Cases Represented by Percentage of Occurrence by Location and the Corresponding Non-TGF Case Reduced to Match TGF Percent and Available Non-TGFs Within the Data Set

Location	Number of Recorded TGF Cases	Percentage of TGFs per Hot Spot Versus Total	Number of Non-TGF Cases Needed Based on Data Set Total	Actual Number of Non-TGF Cases in Data	Non-TGF Data Set (column 3) Reduced to 9940 to Match TGF Percent
Central Africa	26	25.24%	4,482	3,732	2,500
Madagascar	2	1.94%	345	197	180
Oceania	50	48.54%	8,619	8,033	4,730
South Pacific	2	1.94%	345	193	180
Yucatan	23	22.33%	3,965	5,601	2,350
Total	103		17,756		9,940

segregated data that had a known TGF event associated with it via date and time. This data parsing resulted in 103 TGF cases and 17,756 non-TGF cases.

Two investigative methods were chosen to investigate the TGF and non-TGF storm hydrometeor characteristics.

3.1. Geographic Weighting

The net effect of geolocation on hydrometeor content within the TGF-related thunderstorm is the first analysis. Each region has an associated TGF geographic weighting applied. Simply, the weighting is the number of TGFs for that location to the total number of TGFs in the data set. The non-TGF cases were subdivided into each of the five regions. The TGF geographic weighting is applied to the much larger data set for the non-TGF case. The non-TGFs were then randomly selected from that region to match the TGF weighting for that region. Table 3 describes the important elements of the geographic weighting.

For example, central Africa has 26 TGFs (Table 3, column 2) that met Table 2 criteria. One hundred three TGFs compose the complete TGF case data set; therefore, central Africa is 25.24% (Table 3, column 3) of the total data. The non-TGF data set had 17,756 results; this would mean that of these 17,756 points, ideally, 4482 would be from central Africa; however, this is not the case. Only 3732 central Africa non-TGF cases comprise the actual data set (column 5). Table 3, column 6 depicts the final non-TGF cases available based on the geography-weighted TGF of column 3. The same logic is applied to Table 3, rows 2–5. This process resulted in 9940 available non-TGF cases.

3.2. Weighting by LIS Flash Count

The documentation and correlation between lightning flash rate and ice content are well known [*Takahashi*, 1978a, 1978b; *Williams*, 2001; *Williams et al.*, 2005; *Petersen et al.*, 2005]. In this investigation, we look to determine if TGFs are simply some percent of total lightning flashes (referred to as flash count within this paper).

The TGFs cases and non-TGF cases were segregated by the total TGF LIS lightning flash count. Table 4 illustrates the breakdown. Column 1 represents the number of LIS-observed lightning flashes (referred to as flash count) for an event. Row 1, for example, had 11 cases which the observed TGF event contained only one lightning flash. Row 2 (flash count of 2) had 12 TGF cases that had two LIS-observed flashes and so on.

Table 4, column 3 shows the same for total. Column 4 reflects the relative percentage occurrence of TGF events relatively to the total ($n = 103$) for a given flash count. For example, row 1 has 11 TGFs to the total of 103 yielding 10.68%. Column 5 is the number of non-TGF cases extracted from the total number of cases for that particular bin while maintain the same relative percent of column 4. Figure 4 displays this matched distribution. The magnitude of non-TGFs binned is much greater; however, the distributions are equal. The large number of low flash count non-TGF storms was from the Oceania region. To account for this overweighting, a script was run that randomly selected non-TGF cases from each flash count bin. For example, row 1, column 3 has 5760 non-TGF data points, 107 (column 5) were randomly selected from column 3. This process was repeated 100 times and repeated for each row. Column 6 represents the percentage of all non-TGFs events for a particular lightning flash count bin to the total number of non-TGFs events (17,714). This in the non-TGF analog of column 4. Column 7 represents the ratio of the number of TGF cases to the total number of observed LIS flash counts (TGF and non-TGF events). For

Table 4. TGF Lightning Flash Count Distribution With Corresponding Non-TGF Distribution Matched to the TGF Flash Count Percent[a]

Lightning Flash Count	TGFs With Flash Count in Column 1	Non-TGFs With Flash Count in Column 1	Percentage of TGF for Particular FC Bin	Maximum Number of Non-TGFs Which Match TGF Percent	Percentage of Non-TGF for Total	Number of TGFs to Total Flash Count
1	11	5,760	10.68%	107	32.51%	0.001906
2	12	3,276	11.65%	117	18.49%	0.001825
3	6	2,164	5.83%	58	12.21%	0.000922
4	11	1,517	10.68%	107	8.56%	0.001800
5	7	1,124	6.80%	68	6.34%	0.001238
6	8	825	7.77%	78	4.65%	0.001601
7	2	630	1.94%	19	3.55%	0.000452
8	3	473	2.91%	29	2.67%	0.000788
9	7	387	6.80%	68	2.18%	0.001974
10	5	308	4.85%	49	1.73%	0.001597
11	6	258	5.83%	58	1.45%	0.002066
12	6	185	5.83%	58	1.04%	0.002618
13	3	168	2.91%	29	0.94%	0.001350
14	3	136	2.91%	29	0.76%	0.001542
15	2	102	1.94%	19	0.57%	0.001282
16	3	89	2.91%	29	0.50%	0.002038
17	0	63	0.00%	0	0.35%	0.000000
18	1	46	0.97%	10	0.25%	0.001182
19	1	46	0.97%	10	0.25%	0.001120
20	1	33	0.97%	10	0.18%	0.001471
21	1	32	0.97%	10	0.18%	0.001443
22	0	22	0.00%	0	0.12%	0.000000
23	0	18	0.00%	0	0.10%	0.000000
24	0	14	0.00%	0	0.07%	0.000000
25	0	13	0.00%	0	0.07%	0.000000
26	1	14	0.97%	10	0.07%	0.002564
27	2	6	1.94%	19	0.03%	0.009259
28	1	5	0.97%	10	0.02%	0.005952
Total cases	103	17,714	100%	1,001		

[a]Column 6 represents the percent of non-TGF with a particular flash count. Column 7 represents the ratio of TGF cases to the non-TGF case for a particular bin.

example, in row 3, there are six TGF cases with flash count totaling three, and there are 2164 non-TGF cases with this same count; therefore, the ratio is (6 TGF events/(3 × (6 + 2164) flashes).

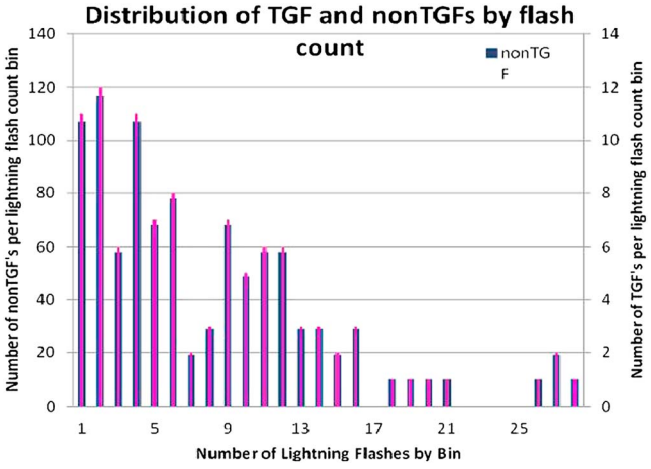

Figure 4. Distribution of TRMM-observed flash count for TGF-related storms with corresponding non-TGF cases matched to the TGF flash count.

4. Results

The hydrometeor results of the two investigative methods are presented. The four graphs (Figures 5–8) represent the maximum concentration (cloud water (CW), cloud ice (CI), precipitation water (PW), and precipitation ice (PI)) distribution of the overall net average of the TGF and non-TGF cases. The graphs represent a reduction of each TGF case and non-TGF case to a single representative-average case for cloud water (CW), cloud ice (CI), precipitation water (PW), and precipitation ice (PI). Standard error bars are included to illustrate the deviation within each averaged data point. *P* value results from a two-tailed *t* test are superimposed over

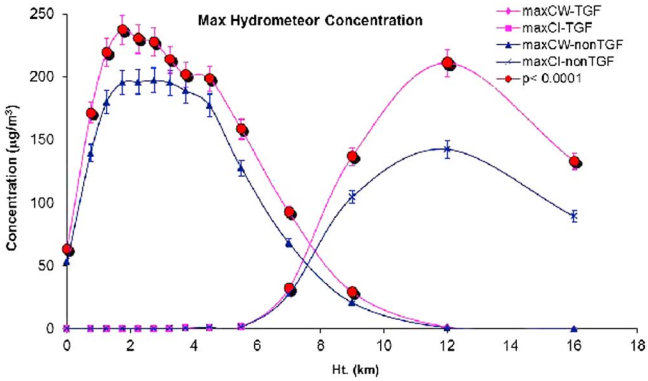

Figure 5. Maximum hydrometeor cloud water and cloud ice distribution of TGF and non-TGF cases referenced to geolocation. Statistically independent data represented by red filled circular overlays.

the data points to reflect either statistically independent or statistically significantly independent data. Typically, statistical independence is defined as a *P* value less than 0.05. Statistically significant difference has a *P* value less than 0.001. Statistically independent data will be represented by red filled circles on the associated TGF data point on Figures 5–8.

4.1. Total Hydrometeor Content Weighted by Regional TGF Distribution

Figure 5 represents the average TGF and non-TGF maximum hydrometeor content (CW and CI) based on the geographic TGF geographic weighting. The TGF stands out dramatically from the non-TGF case for both CW and CI concentrations. Under the assumption that TGFs occur as some small percent of lightning flashes and that flash rate is related to hydrometeor content, Monte Carlo simulations (unshown) showed that significant differences in hydrometeor content between TGF and non-TGF cases could be observed where none should exist. The issues are that TGFs are more likely to be observed when there are a higher number of flashes and hence higher hydrometeor content. This sampling issue can skew the results for TGF cases to higher values.

Minor overlap of error bars does occur for the two case's cloud water data points. The accompanying mixed phase region occurs within the same altitude range for both TGF and non-TGF cases. The respective crossover points appear to occur at the same relative altitude based on TRMM resolution capabilities. The TGF case does possess higher concentrations of CW and CI at the crossover. The crossover is the location of equal water and ice concentrations. The TGF case CI content is nearly 40% greater at peak concentration than the non-TGF case.

Figure 6 represents the maximum precipitation water (PW) and precipitation ice (PI) distribution. Similar to Figure 5, Figure 6 shows a large difference in the TGF PW concentration as compared to the non-TGF case. Only at altitudes above approximately 5 km does PW overlap occurs within the error bars. PI concentrations begin to increase and separate for the TGF case above 5 km and remain greater than the non-TGF PI through maximum observable TRMM altitudes. Mixed phase regions for the two cases are overlapped. As observed in Figure 5, Figure 6's crossover point for the TGF case also occurs at a higher concentration. Non-TGF case PW error bars do overlap with some of the TGF case points.

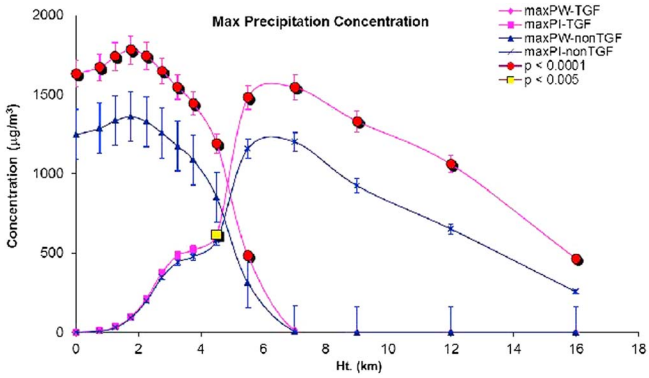

Figure 6. Maximum precipitation water and precipitation ice distribution of TGF and non-TGF cases referenced to geolocation. Statistically independent data represented by red filled circular and yellow filled square overlays.

4.2. Total Flash Count Weighted by TGF Flash Count

The flash count-weighted (as it will be referred to) hydrometeor content CW and CI is different primarily at lower altitudes (1.75 km–4 km), with overlap occurring via the standard error bars; see Figure 7.

In the mixed phase region, the differences are negligible. TGF case CI does peak with minimal overlap

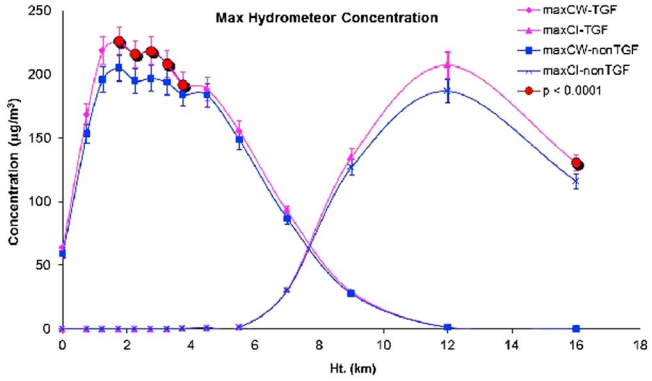

Figure 7. Maximum hydrometeor cloud water and cloud ice distribution of TGF and non-TGF cases referenced to TGF flash count. Statistically independent data represented by red filled circular overlays.

with error bars of the non-TGF case. Figure 8 does present a separation between TGF case and non-TGF case PW concentrations.

Similar to the CW case, they also overlap the standard error bars with the non-TGF case. PI has very little noteworthy difference in concentrations. The flash count-weighted method also indicates the least amount of statistically independent data.

Table 4, column 7 (the ratio of Table 4's column 2 (number of TGF cases with a particular flash count) to column 3 (number of non-TGF cases with the same flash count)) is displayed in Figure 9. The ratio of TGF to total flash count on average is relatively constant (blue bars in Figure 9). Combining the upper bins into one due to the lower number of samples shows a similar trait to the lower bins represented by the red bars (see Figure 9). This supports the conjecture that TGFs may be simply a simple percent of lightning flashes. In addition, the results of section 4.2 may indicate that the significant differences in section 4.1 are largely a result of sampling as suggested by the analytical Monte Carlo simulations noted earlier.

5. Discussion

Two primary questions were pursued with this investigation: Is TGF production merely a function of lightning flash count and does hydrometeor content within the TGF-related storm(s) contains higher concentrations of cloud water, cloud ice, precipitation water, and precipitation ice? Two investigative methods were employed to answer these questions. The TGF case-related and non-TGF case-related storms were categorized according to their total recorded flash count as observed by the LIS instrument aboard the TRMM spacecraft (see Table 4) and their geographic locations (see Figure 1). The results of the hydrometeor comparison based on the geographic weighting did yield results, in which the TGF case storms contained higher concentrations of cloud water, cloud ice, precipitation water, and precipitation ice that were found to be statistically significant. These higher concentrations could be important as it relates to the charging mechanism within the mixed phase region [*Takahashi*, 1978a, 1978b; *Williams*, 2001; *Williams et al*., 2005; *Petersen et al*., 2005] as well as the electric field enhancement [*Gurevich et al*., 1992; *Roussel-Dupré and Gurevich*, 1996; *Gurevich and Zybin*, 2001; *Dwyer*, 2003].

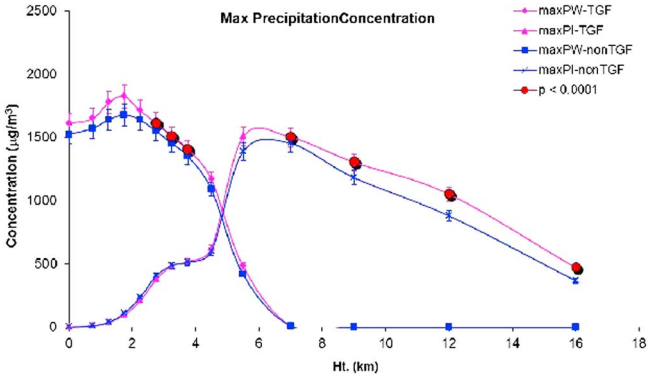

Figure 8. Maximum precipitation water and precipitation ice distribution of TGF and non-TGF cases referenced to TGF flash count. Statistically independent data represented by red filled circular overlays.

On the other hand, analysis weighted by lightning flash count does not show significant differences in the hydrometeor content between TGF and non-TGF data sets. The analysis shown in Figure 9 suggests an important result that TGFs may be a relatively constant fraction of lightning flashes. The differences between the analysis in sections 4.1 and 4.2 may be due to sampling strategy-related issues, and this is an important caveat of the results in section 4.1. Clearly, interesting issues remain in the understanding the geographical differences in convection as they related to lightning flash rates and TGF occurrence.

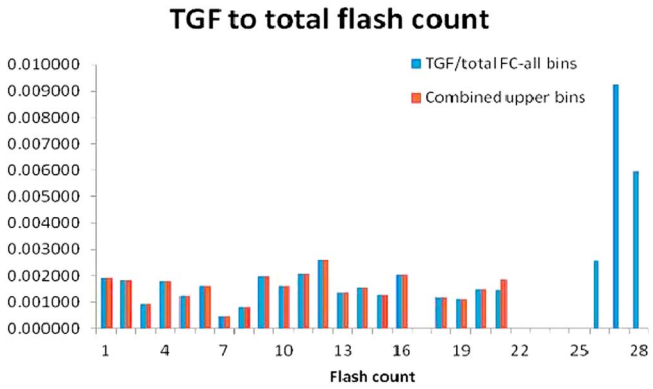

Figure 9. Ratio TGF to total TGF and non-TGF lightning flash count per bin. The results show a considerable increase in TGFs with increase in total lightning flash count.

The TGF case data set contains only 103 cases, and a larger data set is desirable. The results could benefit substantially with additional TGF cases matched to TRMM flight paths as well as matching to WWLLN data sets. The newer "weaker" TGFs produced by *Gjesteland et al*. [2012] would be one source of new TGF cases. Additional TGFs may come from AGILE and FERMI observatories as well. The effects of smaller storms and those nearing the end of their life cycle that may have been filtered out by focusing on maximum statistics should also be investigated. Future investigations may utilize newer TGFs matched to TRMM and WWLLN data to study the characteristics of smaller storms [*Splitt et al*., 2010] and those near the end of their life cycle [*Smith et al*., 2010] and how they compare to similar storms which have not had a detected TGF associated with it.

6. Conclusion

This study presented a comparison of TGF-generating storm systems to a non-TGF-producing set as observed by RHESSI. Differences between TGF-averaged and non-TGF-averaged hydrometeor profiles showed significant differences using geographic weighting/lightning flash count weighting. For the geographic weighting, the TGF case contains more cloud water, cloud ice, precipitation water, and precipitation ice at higher altitudes relative to the non-TGF case storms. However, for the weighting based on flash count, differences in the hydrometeor profiles were insignificant. Sampling strategy can thus produce different outcomes, and further investigation of the geographical differences in convection is warranted. Analysis supports the conjecture that TGFs are a consistent percentage of observed flashes as the rate of TGFs as a function of LIS flash count is relatively constant. Further evaluation of these characteristics will lead to better techniques in identifying storms that may produce a TGF. Identification of TGF-related storms will be beneficial for pilots, flight crews, and passengers aboard aircraft who may be harmed due to the large doses of energetic radiation [*Dwyer et al*., 2010].

Acknowledgments

RHESSI orbital data utilized in this research came from Santa Cruz Institute for Particle Physics and Physics Department, University of California. "The data used in this effort were acquired as part of the activities of NASA's Science Mission Directorate and are archived and distributed by the Goddard Earth Sciences (GES) Data and Information Services Center (DISC) and are freely available at http://science1.nasa.gov/missions/trmm/." This work was supported in part by Robert Holzworth and Michael Hutchins of the Department of Earth and Space Sciences, University of Washington, and the WWLLN data they provided. I would like to thank my fiancée Sherry for her review of this manuscript. I would also like to thank Meagan Schaal for her discussions and review of this work. This work was supported in part by DARPA grant HR0011-08-1-0088 and HR0011-1-10-1-0061.

References

Bonk, J. (2008), README Document for TRMM 2A12, Version 006 GES DISC, NASA Goddard Space Flight Center.

Briggs, M. S., et al. (2010), First results on terrestrial gamma ray flashes from the Fermi Gamma-ray Burst Monitor, *J. Geophys. Res.*, *115*, A07323, doi:10.1029/2009JA015242.

Burroughs, W. J., R. Crowder, T. Robertson, E. Vallier-Talbot, and R. Whitaker (2000), *Weather*, Time-Life, Sydney, Australia.

Carlson, B. E., N. G. Lehtinen, and U. S. Inan (2010), Terrestrial gamma ray flash production by active lightning leader channels, *J. Geophys. Res.*, *115*, A10324, doi:10.1029/2010JA015647.

Christian, H. J., et al. (1998), The Lightning Imaging Sensor, Digital media, GHRC DAAC, Huntsville, Ala.

Cummer, S. A., Y. Zhai, W. Hu, D. M. Smith, L. I. Lopez, and M. A. Stanley (2005), Measurements and implications of the relationship between lightning and terrestrial gamma ray flashes, *Geophys. Res. Lett.*, *32*, L08811, doi:10.1029/2005GL022778.

Dwyer, J. R. (2003), A fundamental limit on electric fields in air, *Geophys. Res. Lett.*, *30*(20), 2055, doi:10.1029/2003GL017781.

Dwyer, J. R. (2008), Source mechanisms of terrestrial gamma-ray flashes, *J. Geophys. Res.*, *113*, D10103, doi:10.1029/2007JD009248.

Dwyer, J. R. (2012), The relativistic feedback discharge model of terrestrial gamma-ray flashes, *J. Geophys. Res.*, *117*, A02308, doi:10.1029/2011JA017160.

Dwyer, J. R., and D. M. Smith (2005), A comparison between Monte Carlo simulations of runaway breakdown and terrestrial gamma-ray flash observations, *Geophys. Res. Lett.*, *32*, L22804, doi:10.1029/2005GL023848.

Dwyer, J. R., D. M. Smith, M. A. Uman, Z. Saleh, B. Grefenstette, B. Hazelton, and H. K. Rassoul (2010), Estimation of the fluence of high-energy electron bursts produced by thunderclouds and the resulting radiation doses received in aircraft, *J. Geophys. Res.*, *115*, D09206, doi:10.1029/2009JD012039.

Dwyer, J. R., D. M. Smith, and S. A. Cummer (2012), High-energy atmospheric physics: Terrestrial gamma-ray flashes and related phenomena, *Space Sci. Rev.*, doi:10.1007/s11214-012-9894-0.

Fishman, G. J., P. N. Bhat, R. Mallozzi, J. M. Horack, T. Koshut, C. Kouveliotou, G. N. Pendleton, and C. A. Meegan (1994), Discovery of intense gamma-ray flashes of atmospheric origin, *Science*, *264*, 1313–1316.

Gjesteland, T., N. Østgaard, A. B. Collier, B. E. Carlson, C. Eyles, and D. M. Smith (2012), A new method reveals more TGFs in the RHESSI data, *Geophys. Res. Lett.*, *39*, L05102, doi:10.1029/2012GL050899.

Grefenstette, B. W., D. M. Smith, B. J. Hazelton, and L. I. Lopez (2009), The first RHESSI terrestrial gamma-ray flash catalog, *J. Geophys. Res.*, *114*, A02314, doi:10.1029/2008JA013721.

Grenci, L. M., and J. M. Nese (2002), *World of Weather: Fundamentals of Meteorology*, 3rd ed., Kendall Hunt, Dubuque, Iowa.

Gurevich, A. V., and K. P. Zybin (2001), Runaway breakdown and electric discharges in thunderstorms, *Phys.-Usp.*, *44*(11), 1119–1140.

Gurevich, A. V., G. M. Milikh, and R. Roussel-Dupre (1992), Runaway electron mechanism of air breakdown and preconditioning during a thunderstorm, *Phys. Lett. A*, *165*, 463–468.

Inan, U. S., M. B. Cohen, R. K. Said, D. M. Smith, and L. I. Lopez (2006), Terrestrial gamma ray flashes and lightning discharges, *Geophys. Res. Lett.*, *33*, LI8802, doi:10.1029/2006GL027085.

Kummerow, C., W. Barnes, T. Kozu, J. Shiue, and J. Simpson (1998), The Tropical Rainfall Measuring Mission (TRMM) sensor package, *J. Atmos. Oceanic Technol.*, *15*, 809–817.

Liu, N., and J. R. Dwyer (2013), Modeling terrestrial gamma ray flashes produced by relativistic feedback discharges, *J. Geophys. Res. Space Physics*, *118*, 2359–2376, doi:10.1002/jgra.50232.

Mach, D. M., H. J. Christian, R. J. Blakeslee, D. J. Boccippio, S. J. Goodman, and W. L. Boeck (2007), Performance assessment of the Optical Transient Detector and Lightning Imaging Sensor, *J. Geophys. Res.*, *112*, D09210, doi:10.1029/2006JD007787.

Marisaldi, M., et al. (2010), Detection of terrestrial gamma flashes up to 40 MeV by the AGILE satellite, *J. Geophys. Res.*, *115*, A00E13, doi:10.1029/2009JA014502.

Masunaga, H., T. Iguchi, R. Oki, and M. Kachi (2002), Comparison of rainfall products derived from TRMM microwave imager and precipitation radar, *J. Appl. Meteorol.*, *41*, 849–862.

Moss, G. D., V. P. Pasko, N. Liu, and G. Veronis (2006), Monte Carlo model for analysis of thermal runaway electrons in streamer tips in transient luminous events and streamer zones of lightning leaders, *J. Geophys. Res.*, *111*, A02307, doi:10.1029/2005JA011350.

Petersen, W. A., H. J. Christian, and S. A. Rutledge (2005), TRMM observations of the global relationship between ice water content and lightning, *Geophys. Res. Lett.*, *32*, L14819, doi:10.1029/2005GL023236.

Roussel-Dupré, R., and A. V. Gurevich (1996), On runaway breakdown and upward propagating discharges, *J. Geophys. Res.*, *101*(A2), 2297–2311, doi:10.1029/95JA03278.

Shao, X.-M., T. Hamlin, and D. M. Smith (2010), A closer examination of terrestrial gamma-ray flash-related lightning processes, *J. Geophys. Res.*, *115*, A00E30, doi:10.1029/2009JA014835.

Smith, D. M., L. I. Lopez, R. P. Lin, and C. P. Barrington-Leigh (2005), Terrestrial gamma-ray flashes observed up to 20 MeV, *Science*, *307*, 1085–1088.

Smith, D. M., B. J. Hazelton, B. W. Grefenstette, J. R. Dwyer, R. H. Holzworth, and E. H. Lay (2010), Terrestrial gamma-ray flashes correlated to storm phase and tropopause height, *J. Geophys. Res.*, *115*, A00E49, doi:10.1029/2009JA014853.

Smith, D. M., et al. (2011), The rarity of terrestrial gamma-ray flashes, *Geophys. Res. Lett.*, *38*, L08807, doi:10.1029/2011GL046875.

Splitt, M. E., S. M. Lazarus, D. Barnes, J. R. Dwyer, H. K. Rassoul, D. M. Smith, B. Hazelton, and B. Grefenstette (2010), Thunderstorm characteristics associated with RHESSI identified terrestrial gamma ray flashes, *J. Geophys. Res.*, *115*, A00E38, doi:10.1029/2009JA014622.

Takahashi, T. (1978a), Riming electrification as a charge generation mechanism in thunderstorms, *J. Atmos. Sci.*, *35*, 1536–1548.

Takahashi, T. (1978b), Thunderstorm electrification – A numerical study, *J. Atmos. Sci.*, *41*(17), 2541–2558.

Wang, N.-Y., L. Chuntao, R. Ferraro, D. Wolff, E. Zipser, and C. Kummerow (2009), TRMM 2A12 land precipitation product – Status and future plans, *J. Meteorol. Soc. Jpn.*, *87A*, 237–253, doi:10.2151/jmsj.87A.237.

Williams, E. R. (2001), The electrification of severe storms, *Meteorol. Monogr.*, *28*, 527–528, doi:10.1175/0065-9401-28.50.527.

Williams, E. R., V. Mushtak, D. Rosenfeld, S. Goodman, and D. Boccippio (2005), Thermodynamic conditions favorable to superlative thunderstorm updraft, mixed phase microphysics and lightning flash rate, *Atmos. Res.*, *76*, 288–306.

Wilson, C. T. R. (1925a), The acceleration of beta-particles in strong electric fields, such as those of thunderclouds, *Proc. Cambridge Philos. Soc.*, *22*(4), 534–538, doi:10.1017/S0305004100003236.

Wilson, C. T. R. (1925b), The electric field of a thundercloud and some of its effects, *Proc. Phys. Soc. London*, *37*, 32D–37D, doi:10.1088/1478-7814/37/1/314.

Xu, W., S. Celestin, and V. P. Pasko (2012), Source altitudes of terrestrial gamma-ray flashes produced by lightning leaders, *Geophys. Res. Lett.*, *39*, L08801, doi:10.1029/2012GL051351.